

AR-LIF: ADAPTIVE RESET LEAKY INTEGRATE-AND-FIRE NEURON FOR SPIKING NEURAL NETWORKS

Zeyu Huang, Wei Meng, Quan Liu, Kun Chen and Li Ma*

School of Information Engineering, Wuhan University of Technology, Wuhan, China

ABSTRACT

Spiking neural networks offer low energy consumption due to their event-driven nature. Beyond binary spike outputs, their intrinsic floating-point dynamics merit greater attention. Neuronal threshold levels and reset modes critically determine spike count and timing. Hard reset cause information loss, while soft reset apply uniform treatment to neurons. To address these issues, we design an adaptive reset neuron that establishes relationships between inputs, outputs, and reset, while integrating a simple yet effective threshold adjustment strategy. Experimental results demonstrate that our method achieves excellent performance while maintaining lower energy consumption. In particular, it attains state-of-the-art accuracy on Tiny-ImageNet and CIFAR10-DVS. Codes are available at <https://github.com/2ephyrus/AR-LIF>.

Index Terms— Neuromorphic Computing, Spiking Neural Networks, Spiking Neurons, Neuron Reset Modes

1. INTRODUCTION

As the third generation of neural networks [1], Spiking Neural Networks (SNNs) possess an event-driven nature. They transmit information using 0/1 spikes and enjoy the energy efficiency advantage of multiplication-free inference by converting multiplications into additions [2]. A current research focus is how to achieve performance comparable to or even surpassing that of Convolutional Neural Networks (CNNs) while preserving the event-driven property [3, 4, 5]. Discrete and iterable spiking neuron models [6] have facilitated the development of algorithms for direct training of SNNs [7, 8]. The oversimplification of spiking neuron dynamics [9] and the neglect of spiking neuron heterogeneity [10] are key factors contributing to the suboptimal performance of SNNs. For spiking neurons, different reset modes and threshold levels significantly affect the frequency and number of spikes fired [11]. Neurons employing "hard reset" reset diverse membrane potentials to zero, which reduces the information encoding capability of the network, causes information loss, and

leads to performance degradation [12]. Neurons using "soft reset" have a post-reset potential greater than zero, risking over-activation; moreover, they ignore neuronal heterogeneity, limiting the expressive power of spiking neurons [13].

To address these issues, we propose an adaptive reset leaky integrate-and-fire (AR-LIF) neuron. Based on observations of the simplified soft-reset spiking neuron equation, we find that the output of a spiking neuron is closely related to historical inputs and outputs. Thus, regulating the temporal dynamics of spiking neurons using historical inputs and outputs becomes a reasonable approach. We introduce an additional memory variable into the neuron dynamics, which is responsible for computing nonlinear operations on inputs and outputs. This variable, featuring temporal decay properties, acts as a feedback signal to participate in the neuron's reset process. Additionally, existing reset modes are closely linked to threshold voltage. To enhance the heterogeneity of spiking neurons [14], we express the threshold voltage as a nonlinear function of the input at the same moment, meaning the threshold level is spatiotemporally independent.

Fig. 1 (b) visualizes the neuron outputs, showing that AR-LIF has a lower spike firing rate. Fig. 1 (c) presents the membrane potential distribution of neurons under inputs with perturbed normal distribution. AR-LIF exhibits lower JS divergence and Wasserstein Distance, and according to [15], the greater the difference in the membrane potential distribution of neurons across time steps, the poorer the network performance, it can be inferred that AR-LIF has better performance.

Our proposed method has been validated on multiple static and neuromorphic datasets, achieving state-of-the-art (SOTA) results. Extensive ablation experiments demonstrate the robustness and effectiveness of the proposed model.

2. METHODS

2.1. Leaky Integrate-and-Fire (LIF) Neuron

The discrete and iterative LIF neuron's dynamical equations can be described by three processes:

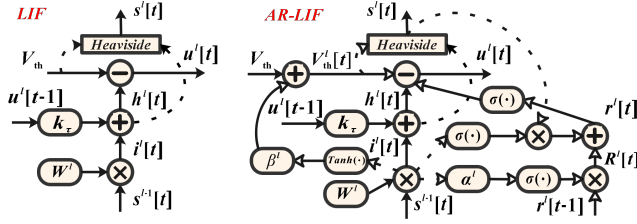
Leaky and integrate: The membrane potential of neurons is composed of the self-decayed membrane potential plus the input current.

$$h^l[t] = k_\tau u^l[t-1] + i^l[t], \quad (1)$$

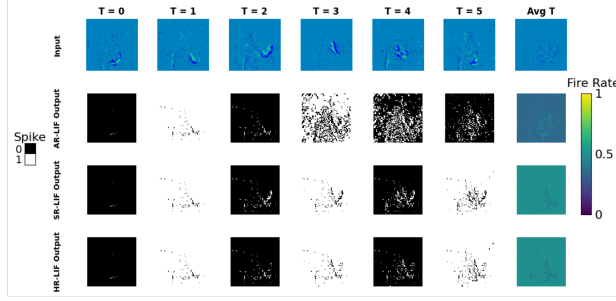
* Corresponding author. excellentmary@whut.edu.cn

This work was supported by National Natural Science Foundation of China (62572364), Natural Science Foundation of Wuhan Municipality (2024040801020263), Science and Technology Talents Serving Enterprise Program of Hubei Province (2025DJB030).

(a) The Structural Description for the vanilla LIF and AR-LIF



(b) Multi-Channel Input Spike Response



(c) Membrane Potential Distribution

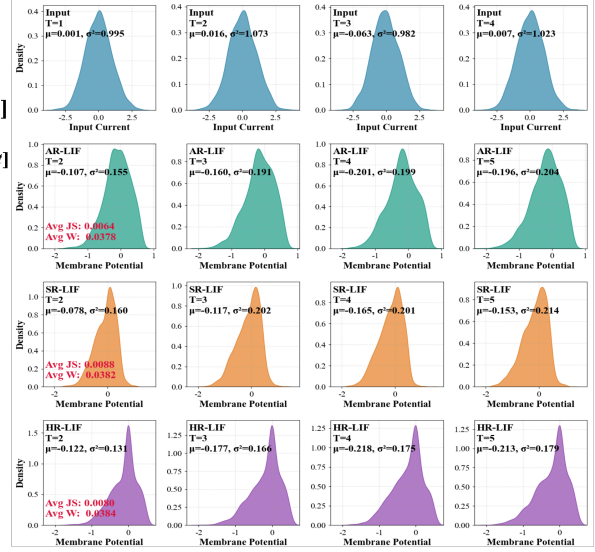


Fig. 1. (a) The hollow arrows in the figure indicate the additional computational processes introduced by AR-LIF. The dashed lines represent the replication of the solid-line outputs of the nodes. (b) Spike responses to 3-channel gesture video inputs. (c) The membrane potential distribution of neurons under inputs with perturbed normal distributions.

where $i^l[t] = W^l * s^{l-1}[t]$, W^l is the synaptic weight, t is time step, and l denotes the l -th layer of the network. $k_\tau \in (0, 1)$ is the neuron membrane decay factor, which is a constant. $i^l[t]$ is the input of the neuron, $u^l[t-1]$ is the membrane potential after spike firing, $h^l[t]$ is the integrated membrane potential, $s^{l-1}[t]$ is the spike output of the neuron.

Fire: When the membrane potential after leaky integration satisfies $h^l[t] > V_{th}$, the output is 1; otherwise, the output is 0.

$$s^l[t] = \Theta(h^l[t] - V_{th}), \quad (2)$$

where $\Theta(\cdot)$ is the Heaviside function, V_{th} is the neuronal threshold.

Reset: After a spiking neuron fires a spike, it needs to reset to restore the voltage to a steady state.

$$u^l[t] = \begin{cases} h^l[t] \odot (1 - s^l[t]), & \text{Hard Reset} \\ h^l[t] - \rho s^l[t], & \text{Soft Reset} \end{cases} \quad (3)$$

where \odot denotes element-wise matrix multiplication. In general, $\rho = V_{th}$, in some studies [13], it is a learnable parameter.

2.2. Motivation of Adaptive Reset Neuron Design

Theorem 1 For a spiking neuron using soft reset, the spike it fires at time t can be expressed as an iterative formula of input and output, independent of the membrane potential.

Proof 2.1 Let the threshold of the neuron be V_{th} , and $u^l[t]$ denotes the membrane potential of the neuron after the spike firing process, and $h^l[t]$ denotes the membrane potential after

leaky integration. We have $h^l[t] = \tau u^l[t-1] + i^l[t]$, $u^l[t] = h^l[t] - s^l[t] \cdot V_{th}$. It can be derived that:

$$\begin{aligned} s^l[t] &= \Theta(h^l[t] - V_{th}) \\ &= \Theta(\tau(h^l[t-1] - V_{th}s^l[t-1]) + i^l[t] - V_{th}) \\ &= \Theta(\underbrace{i^l[t] + \tau i^l[t-1] + \dots + \tau^{t-1} i^l[1]}_{\text{Iterative Formula of Input}} \\ &\quad - \underbrace{V_{th}(1 + \tau s^l[t-1] + \dots + \tau^{t-1} s^l[1])}_{\text{Iterative Formula of Output}}) \end{aligned} \quad (4)$$

Observation 1: Limitations of existing reset modes.

As prior work notes, hard reset's homogeneous mechanism causes significant information loss [12]. Soft reset avoids resetting spiking neurons' potential to 0, instead uniformly subtracting the threshold voltage from them, thus retaining voltage exceeding the threshold but risking excessive activation. Though a learnable parameter ρ enables adaptive adjustment during training, ρ is constrained to positive values [13], leaving the over-activation risk unresolved. Moreover, ρ is shared across neurons in the same layer, lacking neuron-level heterogeneity.

Observation 2: Spiking neurons' output using soft reset is an iteration of inputs and outputs. By Theorem 1, a neuron's spiking at time t is closely linked to cumulative attenuated inputs and spikes from time step 0 to t . Since reset voltage indirectly affects spiking by influencing membrane potential, leveraging cumulative inputs and outputs to construct reset voltage constitutes a viable attempt.

Observation 3: Inspiration from neuronal feedback

regulation mechanisms. Current studies have shown that the excitation and inhibition [16] of biological neurons are closely related to inputs [13]. Therefore, regulating neuronal spike firing using input information is biologically plausible [17].

Based on the above observations on existing neurons, we attempt to design a novel spiking neuron model that integrates an adaptive reset mechanism with a threshold adjustment strategy.

2.3. Adaptive Reset Leaky Integrate-and-Fire Neuron

Adaptive decay of input accumulations: Consider introducing an additional memory variable $r^l[t]$ into the LIF neuron. $r^l[t]$ has an decay property, and the strength of its decay is associated with the input. For negative values of $r^l[t]$, a complementary decay coefficient is adopted. It can be described as:

$$R^l[t] = \begin{cases} \sigma(\alpha^l i^l[t]) \cdot r^l[t-1], & r^l[t-1] \geq 0, \\ (1 - \sigma(\alpha^l i^l[t])) \cdot r^l[t-1], & r^l[t-1] < 0, \end{cases} \quad (5)$$

where $R^l[t]$ denotes an intermediate quantity prior to the accumulation that yields $r^l[t]$, $\alpha^l \in \mathbb{R}$ is a learnable parameter, $\sigma(\cdot)$ is the sigmoid function, $i^l[t]$ is the input at time step t , and $r^l[-1] = 0$.

Spike feedback calculation of input accumulations: $r^l[t]$ is used to count the input penalty amount related to spikes and the input incentive amount without spikes. For inputs that generate spikes, they are accumulated normally; for inputs that do not generate spikes, reverse accumulation is performed. It can be described as:

$$\begin{aligned} r^l[t] &= R^l[t] + s^l[t] \cdot \sigma(i^l[t]) - (1 - s^l[t]) \cdot \sigma(i^l[t]), \\ &= \begin{cases} R^l[t] + \sigma(i^l[t]), & s^l[t] = 1, \\ R^l[t] - \sigma(i^l[t]), & s^l[t] = 0, \end{cases} \end{aligned} \quad (6)$$

where $s^l[t]$ is the output of the spiking neuron at time step t .

Adaptive reset voltage calculation: To ensure the stability of the reset process, the adaptive reset voltage needs to be adjusted by the input accumulation with the threshold as the reference, which is specifically described as:

$$v_r^l[t] = V_{th}^l[t] + \sigma(r^l[t]), \quad (7)$$

where V_{th} is the neuron threshold, which is usually set to 1. We enable the threshold to undergo small-range adaptive adjustment; specifically, $V_{th}^l[t] = 1 + \beta^l \text{Tanh}(i^l[t])$, $\text{Tanh}(\cdot)$ is the hyperbolic tangent function, $\beta^l \in (-1, 1)$.

The adaptive reset process can be calculated as:

$$u^l[t] = h^l[t] - v_r^l[t] \cdot s^l[t], \quad (8)$$

where $v_r^l[t]$ is the adaptive reset voltage.

AR-LIF neuronal dynamics: The structural description for AR-LIF can be found in Fig. 1 (a). Based on the above

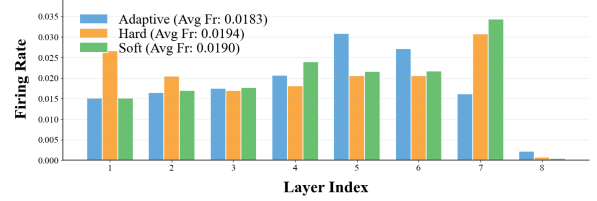


Fig. 2. Firing rates of different neurons across layers.

derivation, the dynamical equations of AR-LIF can be described as follows:

$$\left\{ \begin{array}{l} h^l[t] = k_\tau u^l[t-1] + i^l[t], \\ s^l[t] = \Theta(h^l[t] - V_{th}^l[t]), \\ R^l[t] = \begin{cases} \sigma(\alpha^l i^l[t]) \cdot r^l[t-1], & r^l[t-1] \geq 0, \\ (1 - \sigma(\alpha^l i^l[t])) \cdot r^l[t-1], & r^l[t-1] < 0, \end{cases} \\ r^l[t] = R^l[t] + (2s^l[t] - 1) \cdot \sigma(i^l[t]), \\ v_r^l[t] = V_{th}^l[t] + \sigma(r^l[t]), \\ u^l[t] = h^l[t] - v_r^l[t] \cdot s^l[t], \end{array} \right. \quad (9)$$

where $r^l[t]$ is the self-feedback accumulation of input current.

3. EXPERIMENTS

3.1. Experimental Details

We use the direct training method to train the network, and the loss function is defined based on TET [7].

$$\mathcal{L} = \lambda \mathcal{L}_{\text{TET}} + (1 - \lambda) \mathcal{L}_{\text{MSE}}, \quad (10)$$

where λ is a constant used to control the proportion of each part of the loss function. $\mathcal{L}_{\text{TET}} = \frac{1}{T} \sum_{t=1}^T \mathcal{L}_{\text{CE}}(O(t), y)$, $\mathcal{L}_{\text{MSE}} = \frac{1}{T} \sum_{t=1}^T \text{MSE}(O(t), \phi)$. $O(t)$ is the output of the last layer of the network, and y is the real label value. When \mathcal{L}_{MSE} is used as a regular term, ϕ is a constant; otherwise, it represents the one-hot encoding of the real label value.

We use a rectangular function as a surrogate function to solve the problem of non-differentiability of spike activities in the direct training process:

$$\frac{\partial \mathcal{L}}{\partial W^l} = \sum_{t=0}^T \left(\frac{\partial \mathcal{L}}{\partial s^l[t]} \cdot \frac{\partial s^l[t]}{\partial h^l[t]} + \frac{\partial \mathcal{L}}{\partial u^l[t]} \cdot \frac{\partial u^l[t]}{\partial h^l[t]} \right) \frac{\partial h^l[t]}{\partial W^l}. \quad (11)$$

$$\frac{\partial s^l[t]}{\partial h^l[t]} = \frac{1}{a} \cdot \text{sign}(|h^l[t] - V_{th}| < \frac{a}{2}), \quad (12)$$

where a is set to 1. When $V_{th} - 0.5 \leq h^l[t] \leq V_{th} + 0.5$, $\frac{\partial s^l[t]}{\partial h^l[t]} = 1$; otherwise, $\frac{\partial s^l[t]}{\partial h^l[t]} = 0$.

3.2. Comparisons with Existing Methods

We evaluated the performance of AR-LIF on multiple static and neuromorphic datasets, and the results of their comparison with SOTA methods are presented in Table 1.

Table 1. Compare with previous studies on neuromorphic and static datasets.

Dataset	Method	Architecture	T	Acc.(%)
CIFAR-10	TET[7]	ResNet-19	2/4/6	94.16/94.44/94.50
	GLIF[12]	ResNet-18	2/4/6	94.15/94.67/94.88
	MPD-AGL[18]	ResNet-19	2/4/6	96.18/96.35/96.54
	Ours	ResNet-18	4/6/8	96.1/96.3/96.7
CIFAR-100	GLIF[19]	ResNet-18	6	77.28
	IM-LIF[20]	ResNet-19	3/6	77.21/77.42
	DA-LIF[10]	ResNet-19	1/2/4	79.77/80.59/80.16
	MPD-AGL[18]	ResNet-19	2/4/6	78.84/79.72/80.49
	Ours	ResNet-18	4/6/8	80.1/80.8/81.0
Tiny-ImageNet	IM-LIF[20]	ResNet-19	6	55.37
	MPD-AGL[18]	VGG-13	4	58.14
	LM-H[21]	VGG-13	4	59.93
	CLIF[22]	VGG-13	4/6	63.16/64.13
	Ours	VGG-13	4/6	66.80/67.51
	Ours	VGGSSNN	4/6	68.75/68.93
CIFAR10-DVS	TEBN[8]	VGGSSNN	10	84.9
	DA-LIF[10]	VGG-16	16	82.42
	AGMM[23]	VGGSSNN	10	82.40
	FPT[24]	VGG-11	10	85.7
Ours	VGGSSNN	4/8/16	86.9/87.6/87.9	
DVS-Gesture	MPE-PSN[25]	7B-Net	16/20	97.92/97.22
	DA-LIF[10]	VGG-11	16	98.61
	FPT[24]	VGG-11	20	98.61
	Ours	VGG-11	20	98.61

Table 2. Ablation study. "Both" denotes the scenario where $\alpha^l = 1$ and $V_{th}^l[t] = 1$, while "Learnable" denotes AR-LIF.

Dataset	Accuracy(%)					
	4 Time Steps		Adaptive			
	Hard	Soft	$\alpha^l = 1$	$V_{th}^l[t] = 1$	Both	Learnable
CIFAR100	73.4	63.4	77.0	76.5	76.1	77.8
CIFAR10DVS	83.8	84.1	85.4	84.6	84.3	85.7

CIFAR-10 & CIFAR-100. Compared with GLIF [19], our method remains leading on the ResNet-18 architecture. AR-LIF yields accuracies of 96.7% and 81.0% at time step 8, performing on par with the leading results in SNNs.

Tiny-ImageNet. In comparison with CLIF [22], our method maintains a leading advantage of more than 3% on the VGG-13 architecture. Notably, our method achieves accuracies of 68.75% (T=4) and 68.93% (T=6) on the VGGSSNN architecture, representing the SOTA performance in SNNs.

CIFAR10-DVS [26]. Our method achieves accuracies of 86.9%, 87.6%, and 87.9% at 4, 8, and 16 time steps, respectively. This represents the SOTA result on CIFAR10-DVS.

DVS-Gesture [27]. On the VGG-11, our method can also achieve an accuracy of 98.61% at 20 time steps. This demonstrates the broad effectiveness of our method.

3.3. Ablation Study

To verify the effectiveness of our methods, we performed ablation experiments, with results shown in Table 2. Validation on both static and neuromorphic datasets fully confirms the superiority of AR-LIF and the validity of its dynamic com-

Table 3. The energy consumption for different tasks with the whole testing datasets.

Dataset	Net	T	Params(M)	FLOPs(M)	MACs(M)	ACs(M)	Energy(μ J)
CIFAR-10	ResNet-18	4	11.2	1211.51	1.77	95.65	94.22
CIFAR-100	ResNet-18	4	11.2	1211.60	1.77	96.72	95.19
Tiny-ImageNet	VGGSSNN	4	10.9	4847.11	763.08	209.56	3698.80
CIFAR10-DVS	VGGSSNN	4	9.3	2724.21	428.09	57.35	2020.84
DVS-Gesture	VGG-11	20	9.5	4872.13	1078.11	23.71	4980.63

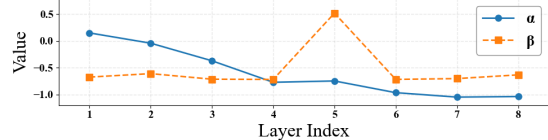


Fig. 3. Tracking of learnable parameters in each layer.

ponents. Specifically, adaptive reset contributes positively, and the threshold adjustment strategy also plays a positive role. Comparative results indicate that threshold adjustment is more critical than the learnability of α^l .

3.4. Analysis of Computational Efficiency

To comprehensively evaluate AR-LIF's performance, we conducted a computational cost analysis with results in Table 3. The energy consumption calculation therein follows [3]. For ease of comparison, experiments on the Gesture dataset were performed with the time step set to 4. As seen in Fig. 2, AR-LIF alters temporal dynamics, causing notable changes in each layer's spike firing rate. Overall, however, it shows a lower average spike firing rate, indicating a slight energy consumption advantage alongside excellent performance.

3.5. Learnable Parameters Tracking

As shown in Equation (9), our method contains two learnable parameters. We visualized the learnable parameters of each layer. The experiment was conducted on the Gesture dataset with T=20, using the VGG-11 architecture. α^l is initialized to 1 and β^l to 0. As shown in Fig. 3, both α^l and β^l have undergone sufficient learning and adjustment, confirming the effectiveness of parameter learnability.

4. CONCLUSION

In this work, we analyze the drawbacks of existing reset modes, and propose a spiking neuron model with adaptive reset, AR-LIF. Adaptive reset leverages accumulated input current and output spikes to dynamically and heterogeneously adjust the reset voltage. Combined with a spatiotemporally independent threshold adjustment strategy, AR-LIF performs excellently on static and neuromorphic datasets while maintaining an energy consumption advantage. Extensive ablation studies further confirm the effectiveness of our method.

5. REFERENCES

- [1] W. Maass, “Networks of spiking neurons: the third generation of neural network models,” *Neural networks*, vol. 10, no. 9, pp. 1659–1671, 1997.
- [2] W. Meng, Z. Huang, Q. Liu, M. Cai, K. Chen, and L. Ma, “Spike-driven inceptionformer: A hierarchical spiking transformer with inception-inspired feature learning,” *Neurocomputing*, vol. 648, pp. 130727, 2025.
- [3] M. Yao, J. Hu, Z. Zhou, L. Yuan, Y. Tian, B. Xu, and G. Li, “Spike-driven transformer,” in *Proceedings of Advances in Neural Information Processing Systems (NeurIPS)*, 2023, vol. 36, pp. 64043–64058.
- [4] M. Yao, X. Qiu, T. Hu, J. Hu, Y. Chou, K. Tian, J. Liao, L. Leng, B. Xu, and G. Li, “Scaling spike-driven transformer with efficient spike firing approximation training,” *IEEE Transactions on Pattern Analysis and Machine Intelligence*, vol. 47, pp. 2973–2990, 2025.
- [5] Z. Zhou, J. Niu, Y. Zhang, L. Yuan, and Y. Zhu, “Spiking transformer with spatial-temporal spiking self-attention,” in *IEEE International Conference on Acoustics, Speech and Signal Processing (ICASSP)*, 2025, pp. 1–5.
- [6] Y. Wu, L. Deng, G. Li, J. Zhu, and L. Shi, “Spatio-temporal backpropagation for training high-performance spiking neural networks,” *Frontiers in neuroscience*, vol. 12, pp. 331, 2018.
- [7] S. Deng, Y. Li, S. Zhang, and S. Gu, “Temporal efficient training of spiking neural network via gradient re-weighting,” in *Proceedings of International Conference on Learning Representations (ICLR)*, 2022.
- [8] C. Duan, J. Ding, S. Chen, Z. Yu, and T. Huang, “Temporal effective batch normalization in spiking neural networks,” in *Proceedings of Advances in Neural Information Processing Systems (NeurIPS)*, 2022, vol. 35, pp. 34377–34390.
- [9] Q. Liu, M. Cai, K. Chen, Q. Ai, and L. Ma, “Reconstruction of adaptive leaky integrate-and-fire neuron to enhance the spiking neural networks performance by establishing complex dynamics,” *IEEE Transactions on Neural Networks and Learning Systems*, vol. 36, pp. 2619–2633, 2023.
- [10] T. Zhang, K. Yu, J. Zhang, and H. Wang, “Da-lif: Dual adaptive leaky integrate-and-fire model for deep spiking neural networks,” in *IEEE International Conference on Acoustics, Speech and Signal Processing (ICASSP)*. IEEE, 2025, pp. 1–5.
- [11] Q. Ai, Y. Yang, M. Cai, K. Chen, Q. Liu, and L. Ma, “A cross-layer residual spiking neural network with adaptive threshold leaky integrate-and-fire neuron and learnable surrogate gradient,” *Knowledge-Based Systems*, vol. 319, pp. 113575, 2025.
- [12] Y. Guo, Y. Chen, L. Zhang, Y. Wang, X. Liu, X. Tong, Y. Ou, X. Huang, and Z. Ma, “Reducing information loss for spiking neural networks,” in *Proceedings of European Conference on Computer Vision (ECCV)*. Springer, 2022, pp. 36–52.
- [13] S. Zhang, Q. Yang, C. Ma, J. Wu, H. Li, and K. Tan, “Tc-lif: A two-compartment spiking neuron model for long-term sequential modelling,” in *Proceedings of the AAAI conference on artificial intelligence (AAAI)*, 2024, vol. 38, pp. 16838–16847.
- [14] S. Wang, T. Cheng, and M. Lim, “Ltmd: learning improvement of spiking neural networks with learnable thresholding neurons and moderate dropout,” in *Proceedings of Advances in Neural Information Processing Systems (NeurIPS)*, 2022, vol. 35, pp. 28350–28362.
- [15] Y. Ding, L. Zuo, M. Jing, P. He, and H. Deng, “Rethinking spiking neural networks from an ensemble learning perspective,” in *Proceedings of International Conference on Learning Representations (ICLR)*, 2025, vol. 2025, pp. 34477–34503.
- [16] D. Zhao, Y. Zeng, and Y. Li, “Backeisnn: A deep spiking neural network with adaptive self-feedback and balanced excitatory–inhibitory neurons,” *Neural Networks*, vol. 154, pp. 68–77, 2022.
- [17] H. Zheng, Z. Zheng, R. Hu, B. Xiao, Y. Wu, F. Yu, X. Liu, G. Li, and L. Deng, “Temporal dendritic heterogeneity incorporated with spiking neural networks for learning multi-timescale dynamics,” *Nature Communications*, vol. 15, no. 1, pp. 277, 2024.
- [18] J. Jiang, L. Wang, R. Jiang, J. Fan, and R. Yan, “Adaptive gradient learning for spiking neural networks by exploiting membrane potential dynamics,” in *Proceedings of International Joint Conference on Artificial Intelligence (IJCAI)*, 2025.
- [19] X. Yao, F. Li, Z. Mo, and J. Cheng, “Glif: A unified gated leaky integrate-and-fire neuron for spiking neural networks,” in *Proceedings of Advances in Neural Information Processing Systems (NeurIPS)*, 2022, vol. 35, pp. 32160–32171.
- [20] S. Lian, J. Shen, Z. Wang, and H. Tang, “Im-lif: Improved neuronal dynamics with attention mechanism for direct training deep spiking neural network,” *IEEE Transactions on Emerging Topics in Computational Intelligence*, vol. 8, no. 2, pp. 2075–2085, 2024.
- [21] Z. Hao, X. Shi, Z. Huang, T. Bu, Z. Yu, and T. Huang, “A progressive training framework for spiking neural networks with learnable multi-hierarchical model,” in *Proceedings of International Conference on Learning Representations (ICLR)*, 2024, vol. 2024, pp. 4925–4941.
- [22] Y. Huang, X. Lin, H. Ren, H. Fu, Y. Zhou, Z. Liu, B. Pan, and B. Cheng, “Clif: Complementary leaky integrate-and-fire neuron for spiking neural networks,” in *Proceedings of International Conference on Machine Learning (ICML)*, 2024, pp. 19949–19972.
- [23] Y. Liang, W. Wei, A. Belatreche, H. Cao, Z. Zhou, S. Wang, M. Zhang, and Y. Yang, “Towards accurate binary spiking neural networks: Learning with adaptive gradient modulation mechanism,” in *Proceedings of the AAAI conference on artificial intelligence (AAAI)*, 2025, vol. 39, pp. 1402–1410.
- [24] W. Feng, X. Gao, W. Du, H. Shi, P. Zhao, P. Wu, and C. Miao, “Efficient parallel training methods for spiking neural networks with constant time complexity,” in *Proceedings of International Conference on Machine Learning (ICML)*, 2025.
- [25] H. Chen, L. Yu, S. Zhan, P. Yao, and J. Shao, “Time-independent spiking neuron via membrane potential estimation for efficient spiking neural networks,” in *IEEE International Conference on Acoustics, Speech and Signal Processing (ICASSP)*. IEEE, 2025, pp. 1–5.
- [26] H. Li, H. Liu, X. Ji, G. Li, and L. Shi, “Cifar10-dvs: an event-stream dataset for object classification,” *Frontiers in neuroscience*, vol. 11, pp. 244131, 2017.
- [27] A. Amir, B. Taba, D. Berg, T. Melano, J. McKinstry, et al., “A low power, fully event-based gesture recognition system,” in *Proceedings of the IEEE Conference on Computer Vision and Pattern Recognition (CVPR)*, 2017, pp. 7243–7252.